AD-A040 938 ROME AIR DEVELOPMENT CENTER GRIFFISS AFB N Y F/G 17/9
MEASURED RESONANT-REGION RADAR SCATTERING BY TRUCKS AND JEEPS.(U)
MAR 77 R B MACK

UNCLASSIFIED RADC-TR-77-98 NL

1 OF 1
ADA040938

END
DATE FILMED
7-77

RADC-TR-77-98
IN-HOUSE REPORT
MARCH 1977

Measured Resonant-Region Radar Scattering by Trucks and Jeeps

RICHARD B. MACK

ROME AIR DEVELOPMENT CENTER
AIR FORCE SYSTEMS COMMAND
GRIFFISS AIR FORCE BASE, NEW YORK 13441

This report has been reviewed by the RADC Information Office (OI) and is releasable to the National Technical Service (NTIS). At NTIS it will be releasable to the general public, including foreign nations.

This technical report has been reviewed and approved for publication.

APPROVED:

PHILIPP BLACKSMITH
Chief, Antenna and Radar Techniques Branch

APPROVED:

ALLAN C. SCHELL, Acting Chief
Electromagnetic Sciences Division

FOR THE COMMANDER:

Plans Office

MISSION
of
Rome Air Development Center

RADC plans and conducts research, exploratory and advanced development programs in command, control, and communications (C^3) activities, and in the C^3 areas of information sciences and intelligence. The principal technical mission areas are communications, electromagnetic guidance and control, surveillance of ground and aerospace objects, intelligence data collection and handling, information system technology, ionospheric propagation, solid state sciences, microwave physics and electronic reliability, maintainability and compatibility.

Printed by
United States Air Force
Hanscom AFB, Mass. 01731

Unclassified

SECURITY CLASSIFICATION OF THIS PAGE (When Data Entered)

REPORT DOCUMENTATION PAGE

READ INSTRUCTIONS BEFORE COMPLETING FORM

1. REPORT NUMBER: RADC-TR-77-98	2. GOVT ACCESSION NO.
3. RECIPIENT'S CATALOG NUMBER	
4. TITLE (and Subtitle): MEASURED RESONANT-REGION RADAR SCATTERING BY TRUCKS AND JEEPS	5. TYPE OF REPORT & PERIOD COVERED: Technical Rept. Inhouse
	6. PERFORMING ORG. REPORT NUMBER
7. AUTHOR(s): Richard B. Mack	8. CONTRACT OR GRANT NUMBER(s)
9. PERFORMING ORGANIZATION NAME AND ADDRESS: Deputy for Electronic Technology (RADC), Hanscom AFB, Massachusetts 01731	10. PROGRAM ELEMENT, PROJECT, TASK AREA & WORK UNIT NUMBERS: 61102F, 2305J403
11. CONTROLLING OFFICE NAME AND ADDRESS: Deputy for Electronic Technology (RADC), Hanscom AFB, Massachusetts 01731	12. REPORT DATE: March 77
	13. NUMBER OF PAGES: 35
14. MONITORING AGENCY NAME & ADDRESS (if different from Controlling Office): 37p.	15. SECURITY CLASS. (of this report): Unclassified
	15a. DECLASSIFICATION/DOWNGRADING SCHEDULE

16. DISTRIBUTION STATEMENT (of this Report)

Approved for public release. Distribution unlimited.

2305 J4

17. DISTRIBUTION STATEMENT (of the abstract entered in Block 20, if different from Report)

18. SUPPLEMENTARY NOTES

19. KEY WORDS (Continue on reverse side if necessary and identify by block number)

Radar cross sections
Backscatter
Phase
Resonance region
Vehicles
Experimental

20. ABSTRACT (Continue on reverse side if necessary and identify by block number)

This report describes measured free-space radar backscatter properties of a 6 × 6 truck with and without a cargo space, and a jeep. Measurements were carried out at 10 GHz on a model scattering range, with models scaled to cover a 10:1 frequency range in the lower resonance region. Both conventional radar cross-section patterns and backscatter phase patterns are presented, as well as curves of dual-frequency phase signatures. Measured

DD FORM 1 JAN 73 1473 EDITION OF 1 NOV 65 IS OBSOLETE

Unclassified

SECURITY CLASSIFICATION OF THIS PAGE (When Data Entered)

309050

20. Abstract (Continued)

results are at horizontal polarization and for elevation angles of 0^{o}, 10^{o}, 20^{o}, and 30^{o}. The measurement procedure is discussed and the results are presented to emphasize changes in scattering due to both frequency and elevation angle.

Preface

The author is pleased to acknowledge the contributions of Mr. A.W. Wojcicki, who performed many of the measurements, and of Mr. J.J. Andriotakis, who assisted both with the measurements and with the construction of the models.

Contents

Illustrations

Illustrations

Tables

Measured Resonant-Region Radar Scattering by Trucks and Jeeps

I. INTRODUCTION

The presence of the earth introduces sufficient complications to the scattered fields of even metal targets that results of full-scale field measurements are frequently difficult to interpret. This is especially true at HF and VHF frequencies where typical radar targets such as trucks have physical dimensions comparable in size to the incident radar wavelength and analytical procedures generally break down for all but the simplest targets even in free space. The purpose of the measurements to be described in this report is to provide a basis for determining changes in radar scattering to be expected from typical targets by themselves throughout the lower resonant region.

The results in Sections 4, 5, and 6 were all measured with the model in simulated free space on a cw model scattering range. Sets of three basic models were scaled to yield results corresponding to full systems operating at 30 MHz, 60 MHz, 120 MHz, 150 MHz, and 300 MHz. Thus, the results cover a 10:1 band in the lower resonant region at harmonically-related frequencies. The measurement frequency was 10.0 GHz, and all measurements were at horizontal polarization.

The three models were a 6×6 truck with no cargo space, the same truck with a cargo space, and a jeep. Gross details judged to be significant in terms of a wavelength at the middle frequencies were included on models of the truck; the

(Received for publication 14 March 1977)

jeep has a complicated interior compartment that was not modeled. At the lower frequencies, at least, a reasonable jeep model is little more than a parallelepiped scaled to the correct dimensions, and this is the shape used for the measurements. Thus, all three models are good representations of the real object up to about 150 MHz, and they still provide the gross scattering characteristics correctly at 300 MHz.

In order to provide a basis for estimating distortions of the scattering pattern caused by a tree in the vicinity of the truck, solid nylon rods were used to construct a model corresponding to a tree of 52-ft height and 20-ft branch spread at 120 MHz, and this was measured in various positions relative to the 120-MHz truck model.

The results in Section 4 are arranged to provide ready estimates of the changes in radar cross section due to changes in either the frequency or the depression angle. The absolute radar cross section is given as a function of aspect angle at both the measurement frequency and simulated frequency. The phase and dual-frequency phase signature for both the truck and jeep models at 30 MHz and 60 MHz are given in Section 6.

For a given combination of earth and polarization, principal changes in the radar scattering patterns caused by the presence of the earth occur in the elevation pattern. In addition, at frequencies corresponding to the lower resonant region, the target may be considered to approximate a point scatterer with respect to the effects of the earth, so that the total backscattered field is of a product form with one factor due to the scatterer and one due to the earth. Thus although absolute values may differ, the relative shape of backscatter patterns, recorded as functions of azimuth angle at constant elevation angles, in Section 4, should bear a reasonable qualitative resemblance to full-scale radar measurements of similar targets on the earth.

2. MEASUREMENT EQUIPMENT AND TECHNIQUES

Measurements were carried out at the RADC/ETE Ipswich Radar Reflections Measurement Facility using an X-Band cw balanced TEE backscatter equipment.[1, 2] A block diagram of the equipment is given in Figure 1; a sketch of the microwave anechoic chamber and model mount is given in Figure 2; and one of the models

1. Blacksmith, P., Hiatt, R.E., and Mack, R.B. (1965) Introduction to radar cross section measurements, Proc. IEEE 53:901-920.
2. Mack, R.B., Wojcicki, A.W., and Andriotakis, J.J. (1973) An Implementation of Conventional Methods of Measuring the Amplitude and Phase of Backscatter Fields, AFCRL-TR-73-0418.

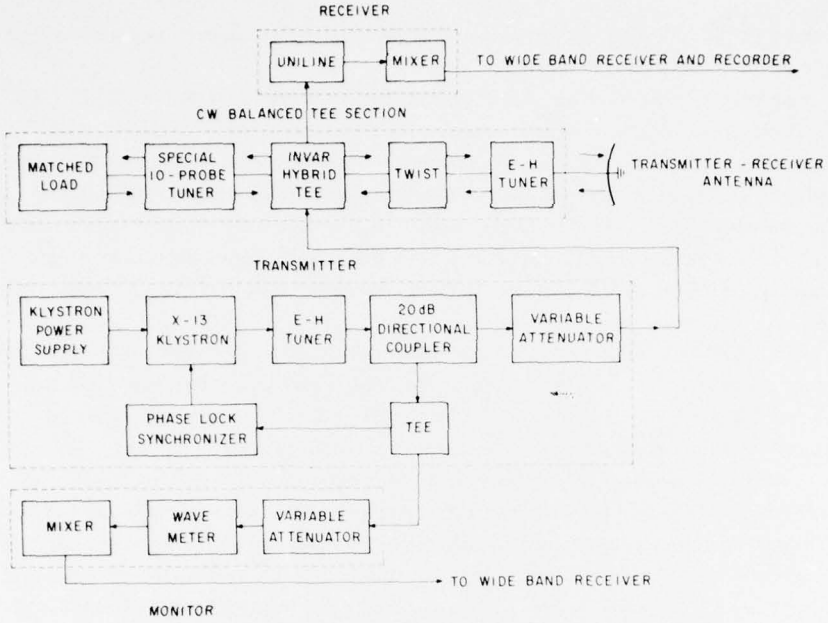

Figure 1. Measurement Equipment

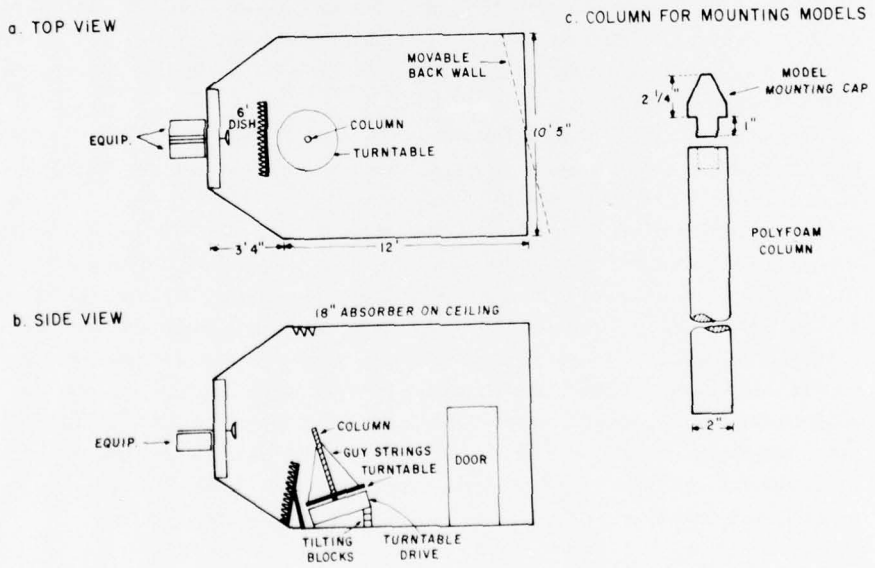

Figure 2. Microwave Anechoic Chamber and Model Mount

mounted in the chamber for measurement of scattering patterns at an elevation angle of 30^{o} is shown in Figure 3.

The transmitter section of this equipment consisted of a Varian X-13 tube stabilized by an FEL Model 133-A phase lock synchronizer. The X-13 was matched through an E-H waveguide tuner for maximum power output. As indicated in Figure 1, the single transmit-receive antenna was a paraboloidal reflector of 6-in. diameter with a double dipole feed. This gave a half-power beam width of about 12^{o}. A Scientific Atlanta Model 1710 Wide Band Receiver and a Scientific Atlanta Model APR 20/30 Pattern Recorder were used to detect and record the data.

Although the measurement equipment was basically a conventional cw backscatter system, several precautions in its design and in the measurement procedure were helpful in reducing the rather high sensitivity of the equipment to changes in room temperature. The central waveguide hybrid tee was made of Invar; all of the waveguide components were wrapped in 1/2 to 1 in. thick slabs of Styrofoam; and the air intake for cooling the X-13 tube was located near the floor.

Cancellation of background signals with the model absent was accomplished by a combination of the E-H tuner next to the antenna and a special 10-probe matching unit (Figure 1). Typically, the E-H tuner was used for the first 40 to 60 dB of cancellation, with the remainder and critical adjustments obtained through the 10-probe unit. The latter had very finely threaded probes to permit small adjustments, and best cancellation times were obtained by adjusting the probes until one of them was relatively insensitive although still providing sufficient reflection to effect the final calcellation.

Measurement periods were limited by the time it took the equipment to drift from a condition of cancelled background signal to a point where this background signal reached its highest tolerable level compared to signal reflected from the target. An adjustment of the fine-tuning probes could normally be obtained so that the equipment always drifted in the same direction from the condition of perfect cancellation. For example, the least sensitive probe might always be used to reestablish the condition of perfect cancellation by rotating it slightly in the counterclockwise direction. Measurement times of 20 to 30 minutes or more could readily be obtained by adjusting the least sensitive probe through its ideal cancellation position and to the maximum tolerable unbalanced condition beyond. The equipment then drifted through the ideal cancellation condition and to the maximum error level beyond, yielding a period for measurements during which errors due to the background signal were always less than some specified level.

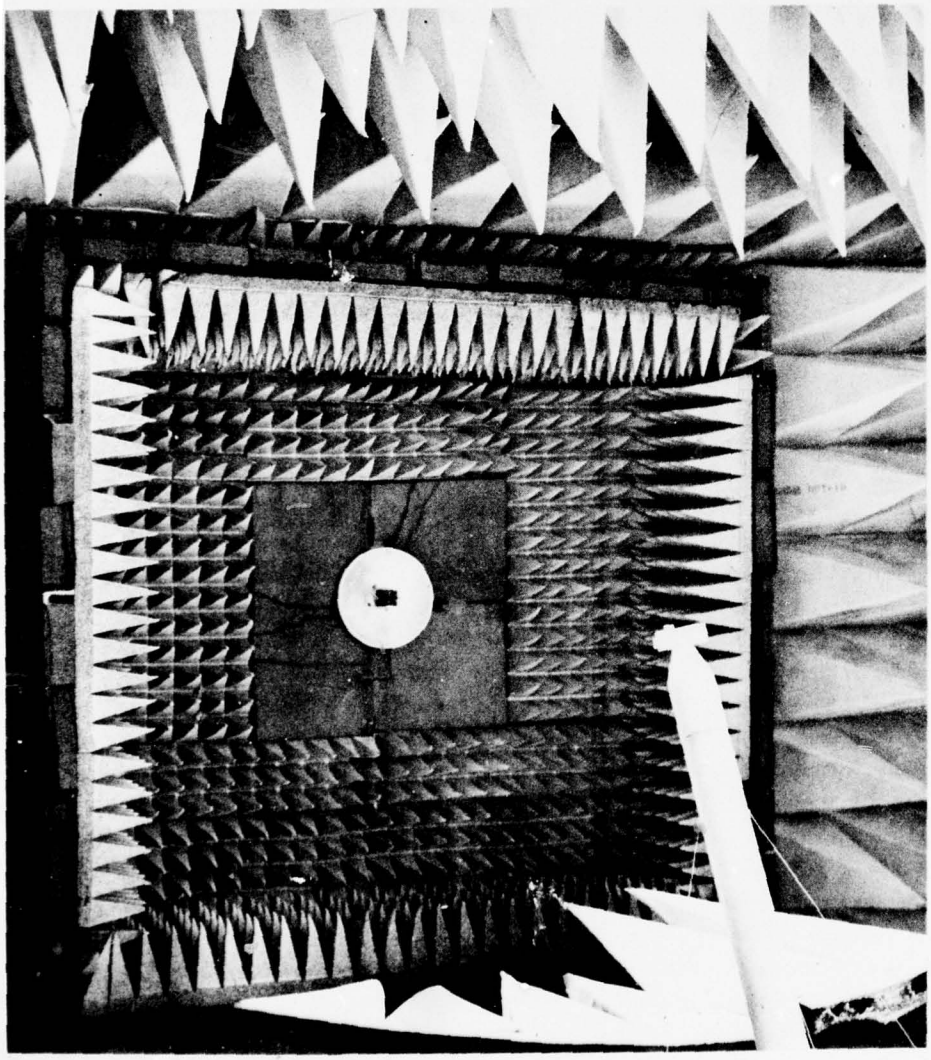

Figure 3. Mounted Model for Measurements at 30° Elevation

The free space chamber (Figure 2) in which these measurements were made is approximately 15 ft long, tapered at the antenna end, and lined with 18-in. pyramidal absorber except over a removable surface near the antenna. Here 1 in. thick AN/75 absorber is used directly behind the antenna with 4-in. pyramidal absorber covering the remainder of this section. The back wall of the chamber can be rotated to direct minimum reflected energy toward the antenna. Models for the present measurements were supported on a Styrofoam column approximately 2 in. in diameter with supporting thin lines attached near the floor to a plywood disk that formed the base of the mount and rotated with the column. The diameter of the Styrofoam column was tuned to yield minimum backscatter at normal incidence at 10.0 GHz. Details of mounting sections designed to permit ready substitution of the models and reference standards are shown in Figure 2c. Models were attached to the top of these sections with small pieces of double-sided transparent tape, and this combination held the models securely in position during rotation on the tilted mount.

The various elevation angles were obtained by tilting the axis of rotation of the mount, Styrofoam column, and model. This was done by resting the edge of the mount farthest from the antenna on fixed sets of blocks to produce elevation angles of 10°, 20°, and 30° as indicated in Figures 2 and 3. Thus, the scattering patterns of Section 4 correspond to identical viewing angles that would occur if an airplane flew circles of constant radius centered about a vertical axis through a fixed target on the earth; elevation angles as given correspond directly to the same depression angles as seen from the airplane. A 0.375-in. diameter metal sphere was used as a reference standard for all of the radar cross-section measurements. At the measurement frequency of 10.0 GHz, this has a cross section of 2.58 cm^2.

The backscatter cross-section measurements of Sections 4 and 5 were carried out with the equipment described in the foregoing paragraphs. For the phase measurements of Section 6, the receiver section of the equipment was modified as shown in Figure 4. The modification consisted in (a) adding an ordinary waveguide tee to the receiver arm of the Invar hybrid in order to split the received signal into two parts; (b) adding a second waveguide hybrid to allow differencing of the scattered signal and of a phase reference signal, derived directly from the transmitter; and (c) adding a precision phase shifter and attenuator to control the phase reference signal. High quality unilines having 30 to 40 dB reverse attenuation were inserted as shown in Figure 4 to eliminate additional spurious reflections and mutual interaction of the branches. With this arrangement, the attenuator and phase shifter in the phase reference line could be adjusted through their complete range of values without disturbing the matched condition of the system. For phase measurements, the Model 1710 Receiver served as a sensitive null detector for indicating when the signal in the phase reference line had been adjusted to be equal in amplitude

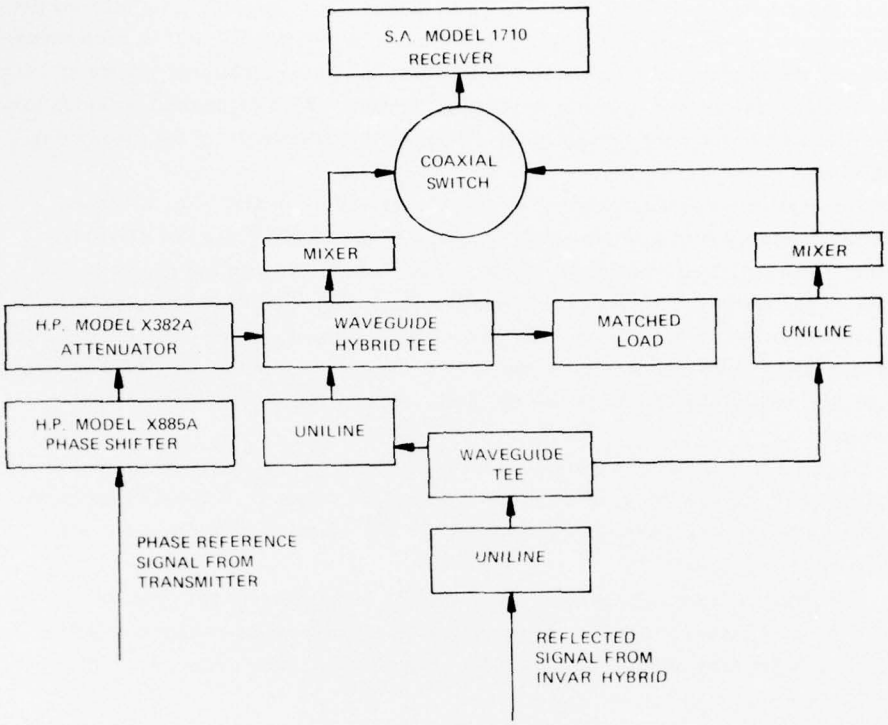

Figure 4. Receiving Section for Phase Measurements

and opposite in phase to the scattered signal in the receiver arm of the second hybrid. Relative phase was determined from settings of the HP Model X885-A phase shifter that produced a null in the receiver. In order to determine more accurately the adjustment of this phase shifter, the setting of the phase shifter that produced equal amplitude readings on either side of the null was read and averaged for each measurement.

Because of the difficulties in locating the model precisely over the rotation axis of the mount, each phase measurement was made at an azimuth angle of θ^{O} and $\theta^{O} + 180^{O}$ with the results averaged to compensate for forward and backward motion of the model as rotated. For models such as the parallelepipeds used to represent jeeps, this was straightforward; for objects having lesser degrees of symmetry such as trucks, the model as well as the mount had to be rotated to present equivalent aspects at θ^{O} and at $\theta^{O} + 180^{O}$. Model rotation for the trucks was accomplished by imbedding a polystyrene pin of 0.003-in. diameter in the

mount and precisely locating small holes in the trucks to provide snug slip-on fits over the pins. When the mount was rotated 180° for the second half of each measurement, the model was also rotated 180° about the pin. Alignment marks on both model and mount served to guide the model rotation. With horizontal polarization, reflections from the polystyrene pin were below the sensitivity of the measuring equipment.

The Styrofoam model mount of Figure 2c was also modified for the phase measurements by cutting a vee along one diameter of the column and carefully mating a vee bottom of the model mount. This served to align the model in one plane. The operator's fingers could easily align the model along the groove in the other plane to within ±0.001 in. Three such model mounts were used – one for the reference standard, one for the models, and one with nothing attached. The empty model mount was placed on the column while background signals were being cancelled.

The reference standard for phase measurements was a thin rod one wavelength long and 0.02 wavelength in diameter. This rod was shown[3,4] to have an effective scattering length with phase of approximately 30°, corresponding to a far-zone field with phase of -150°.

The phase stability of the equipment and the measurement procedures permitted repeated measurements of the reference rod that showed only negligible variations over long periods of time and, in many instances, from day to day.

3. MODELS

Three basic models representing respectively a 6 × 6 truck with no cargo space, a 6 × 6 truck with a cargo space, and a jeep were machined from aluminum in five sizes, with each size chosen according to the linear scaling factors for simulating at the measurement frequency of 10 GHz full-scale vehicles at actual operating frequencies of 30 MHz, 60 MHz, 120 MHz, 150 MHz, and 300 MHz; for example, the 300 MHz model was 300/10,000 or 3 percent of the full vehicle in size. Corresponding to differences in sizes of the full vehicles, the jeep models were approximately 3/4 as wide and 3/4 as high but only half as long as truck models at the same scaling factor.

An open jeep has a complicated passenger compartment with many details that are all at approximately the same structural scale and, hence, difficult to simplify.

---

3. Mack, R.B. (1971) Phase, Phase Signatures, and Simple Inverse Properties of Backscatter Fields from Thin Rods, AFCRL-TR-71-0526.

4. Mack, R.B. (1971) Phase properties of backscattered field from thin rods, IEEE Trans. G-AP AP-19:450-451.

At VHF, these details including the depth of the cockpit are sufficiently small compared to a wavelength that their effect on the over-all scattered fields will be minor. Therefore, in the interests of time and fabrication expense, the jeep was represented by parallelepipeds scaled to the correct over-all dimensions.

A sketch of the more detailed truck model is shown in Figure 5. Dimensions in inches of the actual models are given in Table 1, where dimension labeling corresponds to that of Figure 5. Note that dimensions A, B, C are, respectively, the length, height, and width, and these are used also to specify the jeep. The truck model with no cargo space is the same as shown in Figure 5 but without the space specified by dimensions J, K, L. Figure 6 shows the relative sizes of the models, starting with those scaled for 300 MHz at the top.

The tree was scaled from approximately 120 MHz and constructed of solid nylon rods having a relative dielectric constant of about 3.5, corresponding to wood having a 50 percent moisture content at the measurement frequency of 10 GHz. The choice of dielectric constant was dictated primarily by the ready availability of the nylon rods. The model of the tree was 7-1/2-in. high with branches tapering in length from about 1-1/2-in. at the bottom to 1/2-in. at the top. Rods with diameters of 0.0625-in. were used for the branches; the trunk was untapered and measured 0.250-in. in diameter. Distribution of the branches was pseudo-random.

The tree model is shown in a typical relation to the 120 MHz model truck in Figure 7. The Styrofoam disk shown supporting the tree and truck in Figure 7 was 1-in. thick. It was experimentally tuned for minimum backscatter by reducing its diameter in a lathe in successive steps of 0.050-in. and measuring its reflection after each turning. Several other methods of reducing reflections from the disk, such as shaping its edge, were tried but these proved less effective and were abandoned in favor of the tuning by turning method that readily reduced reflections from the disk to about the balanced background levels of reflection.

A full-sized tree corresponding to the model would have approximately the following characteristics: height - 52 ft, trunk diameter - 2.77 ft, lower branch length - 10.5 ft, and dielectric constant of about 6.5.

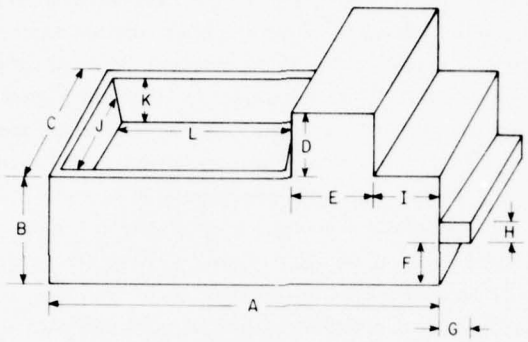

Figure 5. Details of 6 × 6 Truck Models

Table 1. Model Dimensions
(Measuring frequency = 10 GHz)

Operating frequencies: 30, 60, 120, 150, 300 (in megacycles)
Scale factors: 0.0030, 0.0060, 0.0120, 0.0150, 0.0300 (in inches)

Model	Frequency (Mc)				
	30	60	120	150	300
Jeep A	0.243	0.483	0.966	1.209	2.415
B	0.077	0.151	0.302	0.378	0.725
C	0.106	0.215	0.430	0.537	1.075
6 × 6 A	0.406	0.814	1.628	2.038	4.070
B	0.110	0.227	0.454	0.567	1.135
C	0.143	0.286	0.572	0.715	1.430
D	0.036	0.075	0.150	0.188	0.375
E	0.078	0.150	0.300	0.375	0.750
F	0.031	0.062	0.124	0.155	0.310
G	0.030	0.060	0.120	0.150	0.300
H	0.016	0.039	0.080	0.100	0.200
I	0.77	0.160	0.320	0.400	0.800
J		0.185	0.435	0.595	1.310
K		0.125	0.240	0.300	0.600
L		0.390	0.906	1.125	2.320

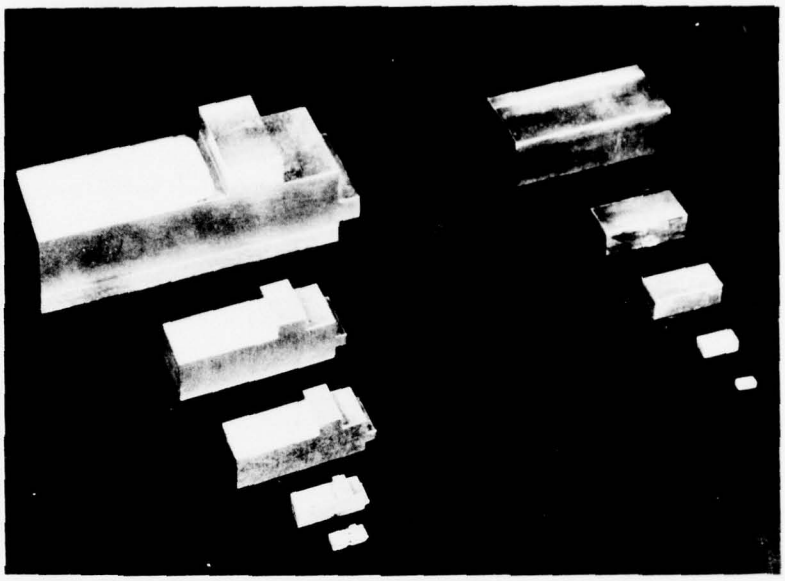

Figure 6. Models Showing Relative Sizes

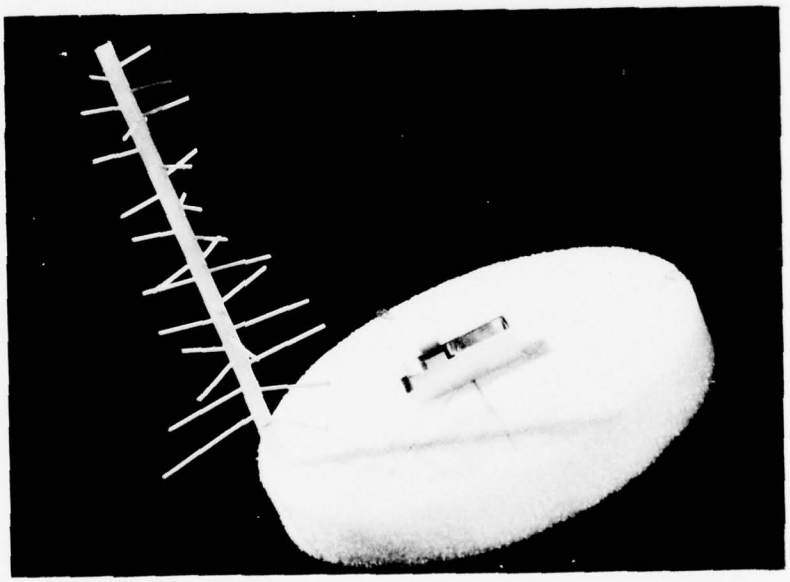

Figure 7. Tree and Truck Models

4. RADAR CROSS SECTIONS OF ISOLATED MODELS

Normalized backscatter patterns for the three models are presented in Figures 8, 9, and 10, where the individual patterns are arranged to exhibit changes in radar cross section (rcs) due to frequency up the page and changes due to elevation angle across the page. In the figures, "Jeep No. 1" refers to the single simplified model of the jeep that was investigated; "Truck No. 1" refers to the truck without a cargo space; and "Truck No. 2" refers to the truck with a cargo space. For the latter, model measurements were carried out only at simulated frequencies of 120 MHz, 150 MHz, and 300 MHz where the depth of the cargo space was a significant fraction of a wavelength.

The radar cross section of the model at the measurement frequency of 10 GHz is given in decibels relative to one cm^2 at the left of each scattering pattern, and the equivalent rcs of the full vehicle at the indicated operating frequency is given in decibels relative to one square meter at the right of each pattern. The rcs at the measurement frequency was determined by measuring the power received from a known reference standard located at the center of the space occupied by the model at the completion of each pattern recording. To find the equivalent rcs at the simulated operating frequency, the known cross section of the standard is scaled by a factor of the square of the ratio of the simulated frequency to the measurement frequency. Thus,

$$\sigma_s = (\lambda_s/\lambda_m)^2 \, \sigma_m \tag{1}$$

and

$$\sigma_{dB} = 10 \log \sigma \tag{2}$$

where σ_m and λ_m are, respectively, the rcs and the wavelength at the measurement frequency, and σ_s and λ_s are the rcs and wavelength at the operational frequency being simulated. If the model actually measured is chosen to be (λ_m/λ_s) of the full vehicle in size, σ_s as scaled by Eq. (1) will be the rcs of the full vehicle at the operating frequency of f_s.

The models were arranged in azimuth so that the rcs of the front of the model occurs at 0^o and that from the side at 90^o in each of the patterns. However, some errors in alignment are evident in the patterns. For example, in Figure 8a the pattern for 300 MHz is shifted to the right by about 22^o so the front actually occurs at 22^o instead of 0^o. In any case, all of the patterns should be symmetrical about the front and rear of the models and these aspects occur near 0^o and 180^o, respectively, so that small shifts should be apparent.

Based on measured background levels and variations in repeated patterns with the models at different locations, the higher cross sections for all but the smallest models should be accurate to well within ±1/2 dB; for the 30 MHz truck this reduces to about ±1 dB, while for the 30 MHz jeep it is reduced further to ±2 dB.

Some interesting general characteristics are readily evident from the patterns. For example, fine structure details of these targets do not show up in the patterns at frequencies below about 120 MHz. Thus, the truck pattern at 60 MHz (Figure 9a) is nearly identical to the jeep pattern at 120 MHz (Figure 8a). Similarly, the truck pattern at 30 MHz is nearly the same as that of the jeep at 60 MHz. In these examples, the factor of 2 in frequency occurs because corresponding models of the truck are approximately twice as long as those of the jeep. Also, the jeep at 60 MHz and the truck at 30 MHz are both approximately $2\lambda/5$ in length, and yield scattering patterns that in shape are much like those that would occur from a thin rod of about the same length. The height and width of both of these models is sufficiently small compared to a wavelength to have little effect on the shape of the scattering pattern.

Generally, the higher elevation angles yield simpler scattering patterns in which much of the fine structure detail has disappeared and in which many of the high maxima due to broadside specular reflections no longer occur. These trends are particularly evident with the 300-MHz truck models for which the patterns at 0° elevation are much more complicated than those at 30° elevation (see Figures 9a and 9d, for example).

For the smaller models, changes in the backscatter pattern due to changes in elevation angle depend primarily on the height and width of the model compared to the incident wavelength, since the principal scattering sources at horizontal polarization are the discontinuities at the longitudinal corners of the models. Thus, any significant interference effects due to the edges are beyond the 30° elevation interval for jeep models through the 120-MHz size, but begin to appear within the 20° to 30° interval for the 150-MHz model. Similarly, interference effects due to changes in the elevation angle start closer to the 0° angle as models increase in size, so that significant changes occur just beyond 10° in elevation for the 300-MHz models.

A comparison of Figures 9 and 10 shows that for truck models through 150 MHz in scale size, there are no changes in the scattering patterns through the first 20° in elevation and only limited changes in the 30° pattern between models that have cargo spaces and those that do not. For the 300-MHz models, differences due to the cargo spaces are evident in the 20° pattern, and become quite pronounced in the 30° pattern.

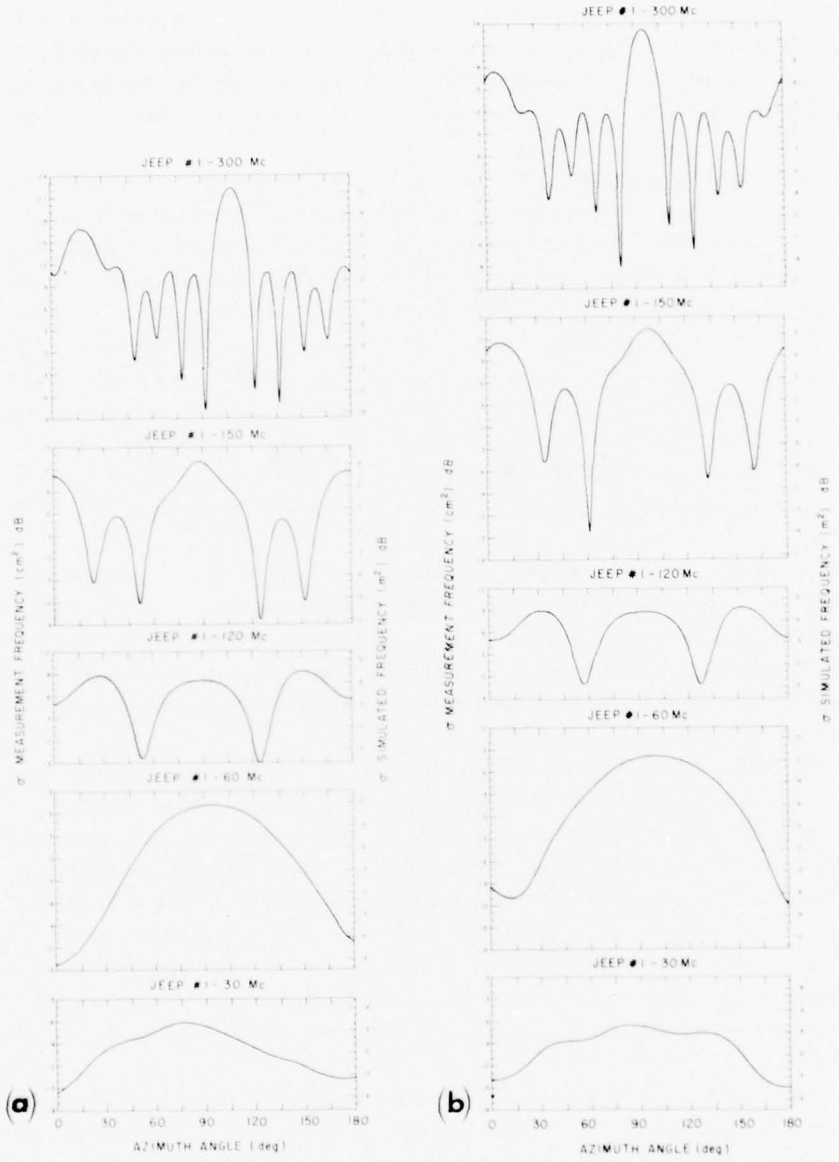

Figure 8. RCS – Jeep. (a) at 0^{O} elevation, (b) at 10^{O} elevation, (c) at 20^{O} elevation, (d) at 30^{O} elevation

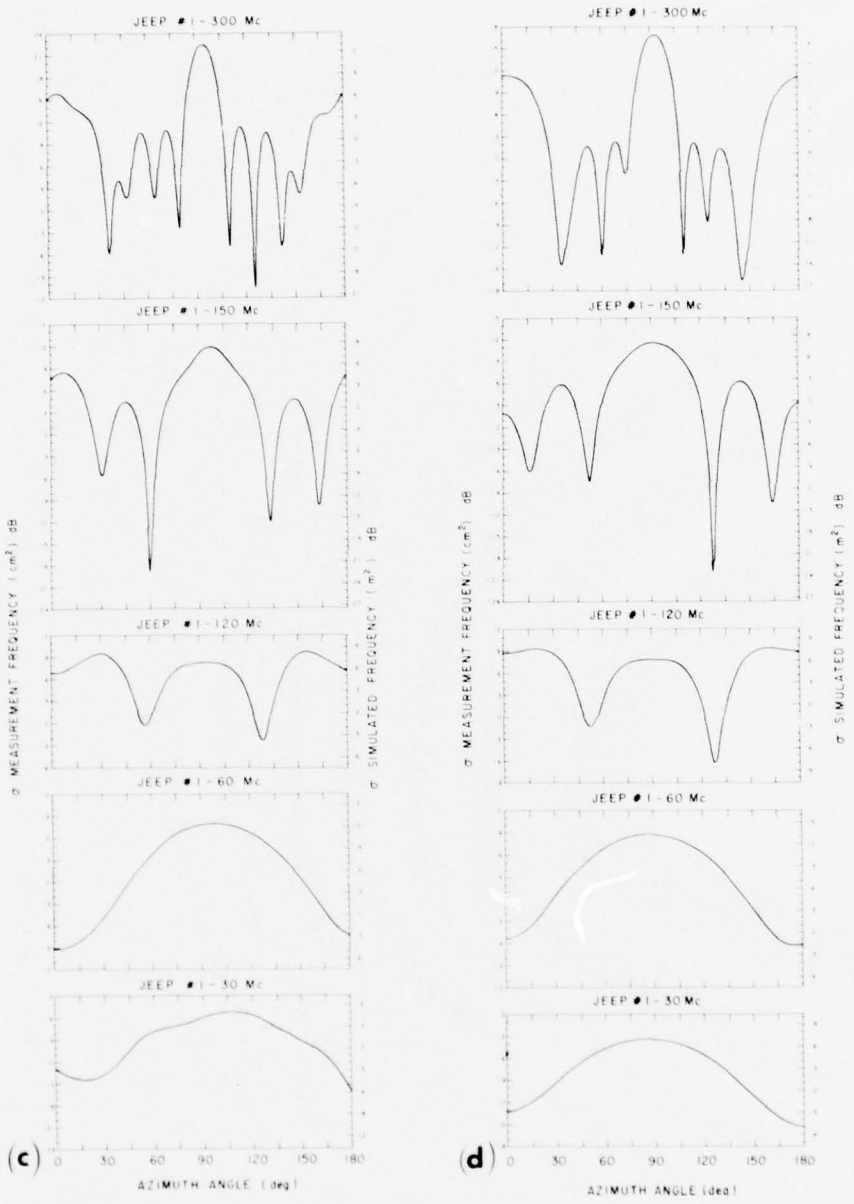

Figure 8. RCS – Jeep. (a) at 0^{O} elevation, (b) at 10^{O} elevation, (c) at 20^{O} elevation, (d) at 30^{O} elevation (Cont.)

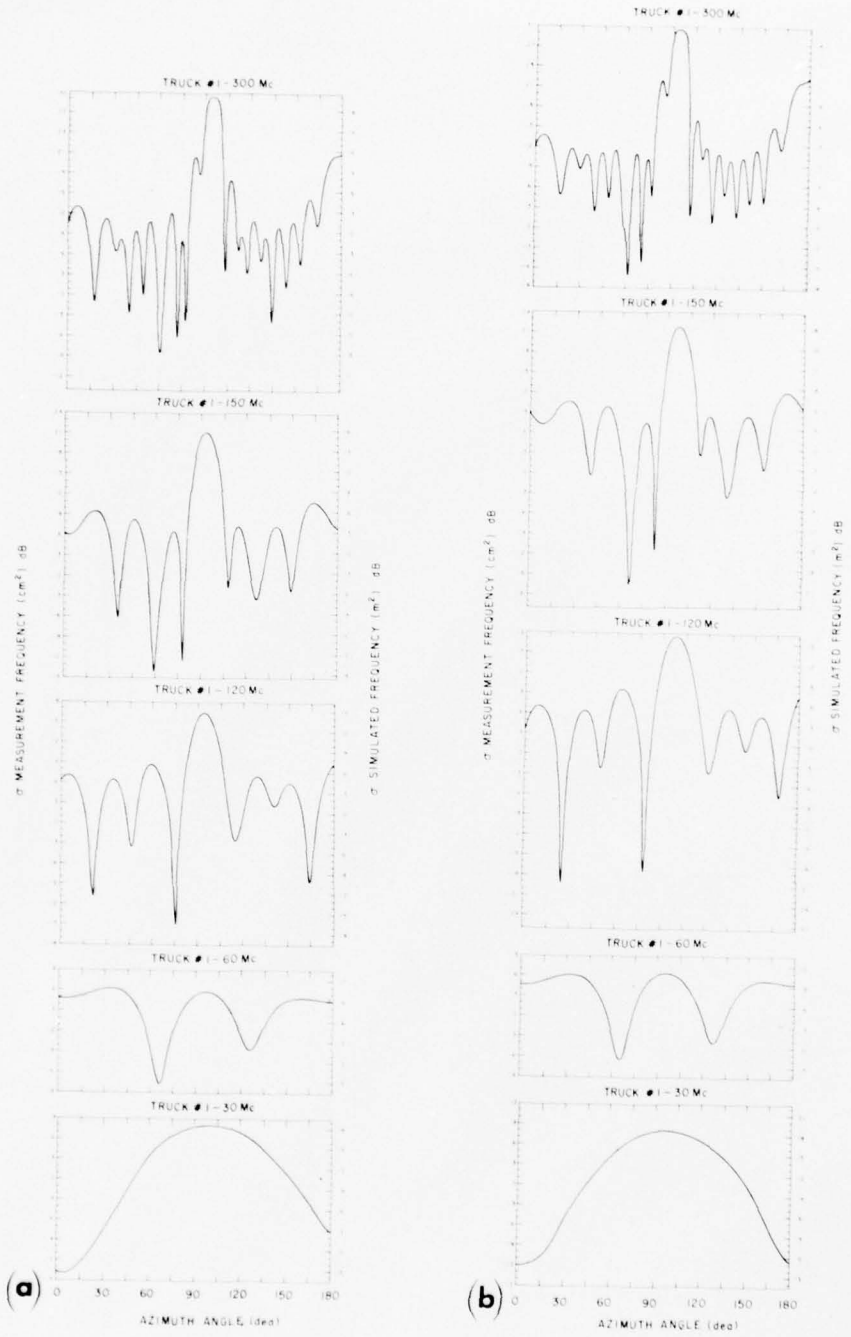

Figure 9. RCS – Truck without Cargo Space. (a) at 0^{o} elevation, (b) at 10^{o} elevation, (c) at 20^{o} elevation, (d) at 30^{o} elevation

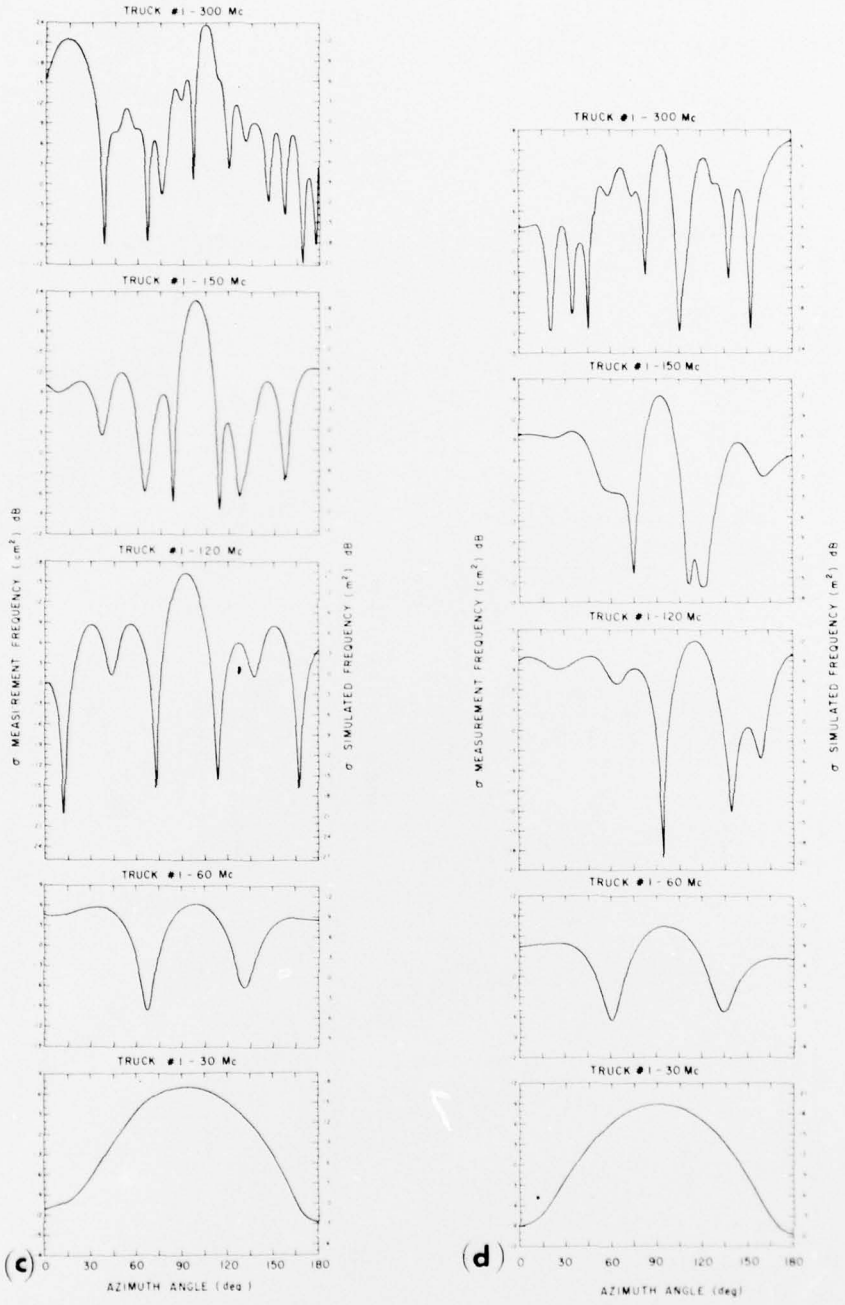

Figure 9. RCS – Truck without Cargo Space. (a) at 0^{O} elevation, (b) at 10^{O} elevation, (c) at 20^{O} elevation, (d) at 30^{O} elevation (Cont.)

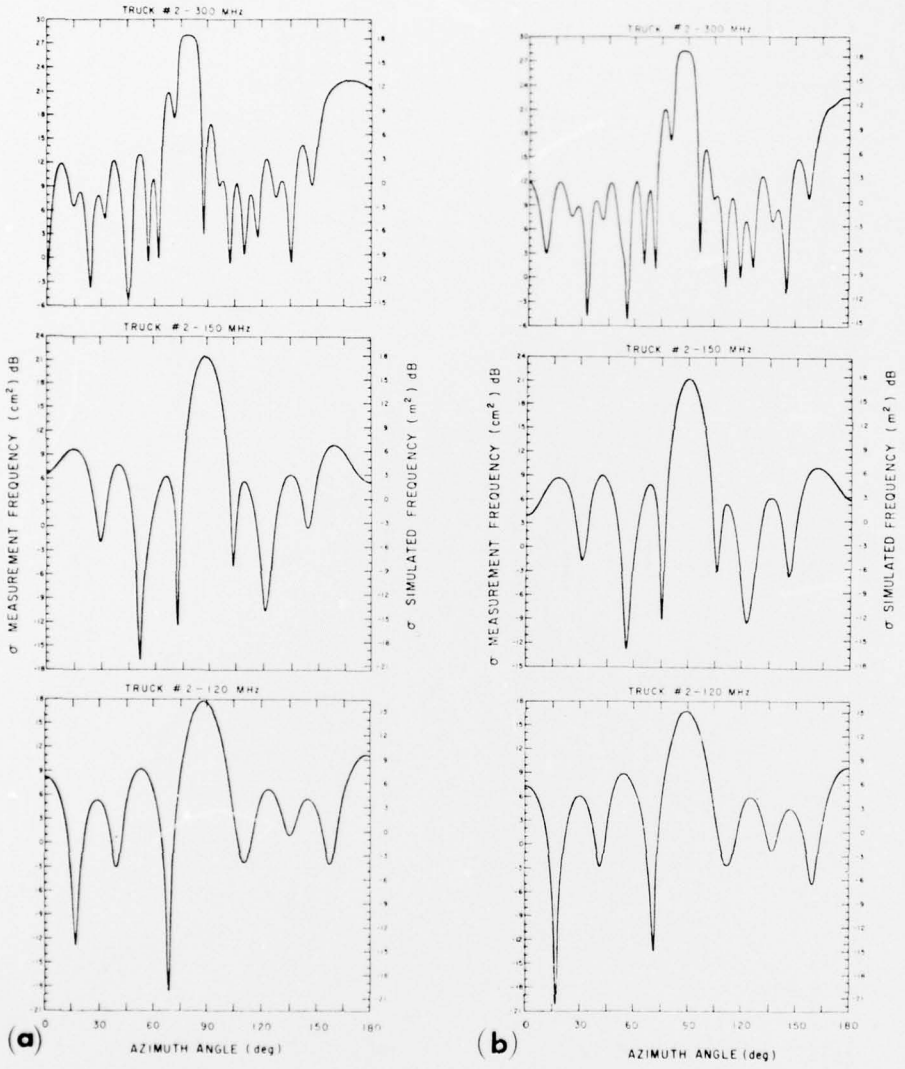

Figure 10. RCS – Truck with Cargo Space. (a) at 0^{O} elevation, (b) at 10^{O} elevation, (c) at 20^{O} elevation, (d) at 30^{O} elevation

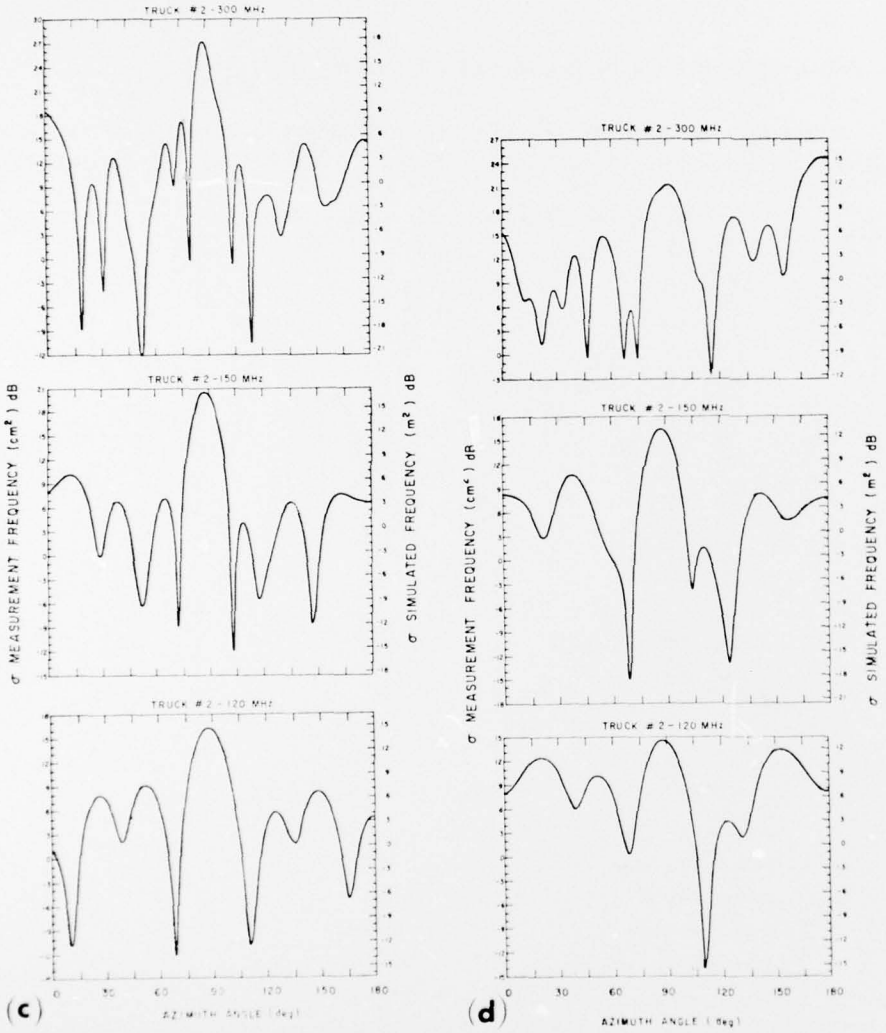

Figure 10. RCS – Truck with Cargo Space. (a) at 0^{O} elevation, (b) at 10^{O} elevation, (c) at 20^{O} elevation, (d) at 30^{O} elevation (Cont.)

The depth-to-width ratio of the cargo space was approximately 0.458; therefore, direct illumination of the interior corner occurs at elevation angles greater than about $\alpha = \tan^{-1} 0.458 = 24.6^{\circ}$, and for model sizes sufficiently large that if the cargo space dimensions are significant fractions of a wavelength, significant changes in the scattering patterns may be expected to occur at elevation angles greater than about 25°, as shown in the measurements.

5. RADAR CROSS SECTIONS OF THE TRUCK MODEL NEAR A TREE

Three sets of backscatter patterns corresponding to three different distances between the truck and tree are given in Figure 11. These patterns have the same

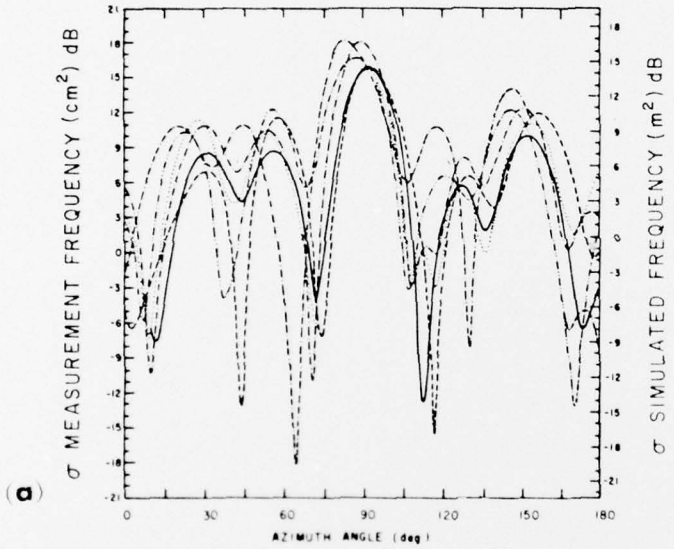

Curve	Azimuth Position of Tree
————	Isolated Truck, No Tree
- - - - - -	0°
—•—•—•—	45°
••••••••••••	90°
—··—·—··—·—	135°
— — · — — · —	180°

(Azimuth Angles from Front of Truck)

Figure 11. RCS – Truck Model 2 Near Tree. Truck-to-tree distance (a) 0.84 λ, (b) 1.70 λ, and (c) 2.5 λ

general format as those discussed in Section 4, with the radar cross sections in decibels relative to one square centimeter at the measurement frequency of 10 GHz given at the left and the radar cross sections in decibels relative to one square meter scaled to the actual operating frequency given at the right. The front of the vehicle is near 0^{O} azimuth in each.

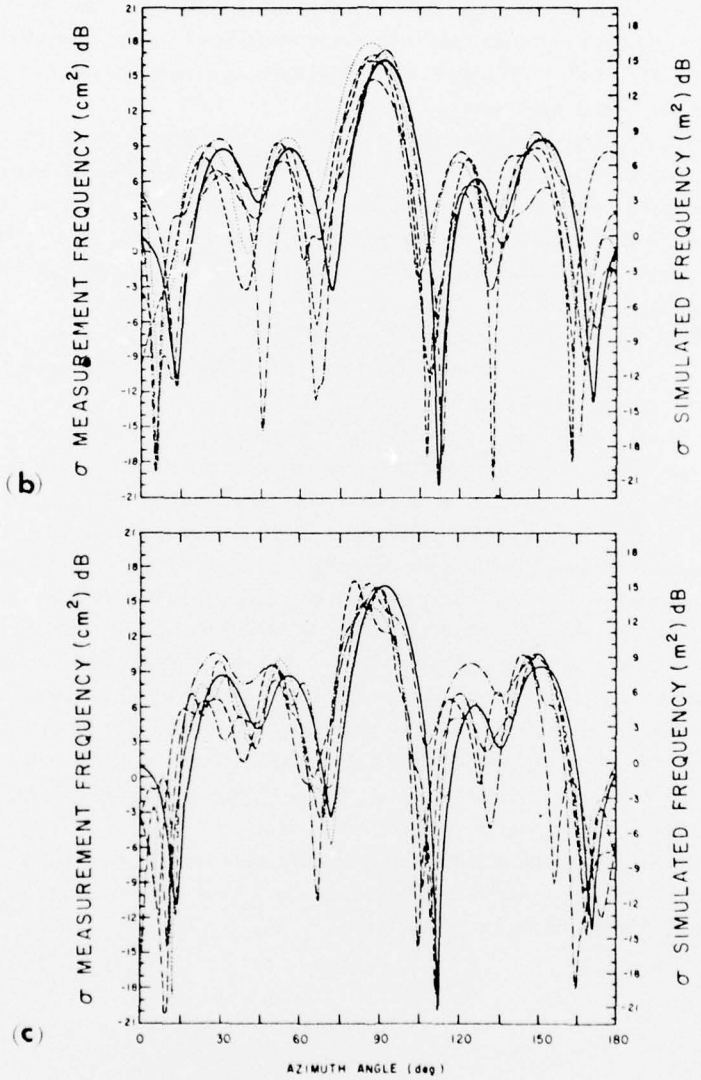

Figure 11. RCS – Truck Model 2 Near Tree. Truck-to-tree distance (a) 0.84 λ, (b) 1.70 λ, and (c) 2.5 λ (Cont.)

All of the patterns are for the 120-MHz model truck with a cargo space, and all are at 20^{O} elevation. At this elevation angle, the truck was shaded by at least several of the horizontal tree branches for each position of the tree.

Distances between the tree and truck are 0.84 λ, 1.70 λ and 2.50 λ, respectively, *in parts* (a), (b) and (c) of Figure 11. For a full system operating at 120 MHz, these distances correspond to approximately 7 ft, 14 ft, and 21 ft, respectively. For each distance, patterns were recorded with the tree at the five locations of 0^{O}, 45^{O}, 90^{O}, 135^{O}, and 180^{O}. The pattern of the isolated truck is given as the solid line in each set.

The tree may be expected to exert its strongest influence on the scattering pattern of the truck when the tree is located directly between the truck and the radar. For a given pattern, this occurs when the azimuth angle of the pattern coincides with the tree location for that particular pattern. Thus, in a pattern for a tree location of 135^{O}, the tree will be directly between the radar and truck at an azimuth angle of 135^{O}.

Except when the tree is located at 0^{O} or 180^{O}, the patterns no longer have any symmetry. However, for presentation ease, only the 180^{O} segment for which the tree directly shades the truck is shown.

As might be expected, the largest changes in patterns occur when the tree is closest to the truck and for directions in which the truck has smallest backscatter cross section. No major new lobes were introduced by the tree, but in several cases pairs of lobes having only 3-to 5-dB dips between them for the isolated truck were changed by the tree into distinct lobes with large dips between them. The lobes were also shifted in azimuth somewhat by the tree but the shift was generally minor. Changes due to the tree in directions of the front and rear of the truck were quite large for all positions of the tree. Here, total variations of at least 10 dB can commonly be seen as the tree position was changed.

Pattern changes due to the tree were generally much smaller for the 2.5 λ separation. Here, although the largest changes still occur in the low power directions toward the front and rear of the truck, some changes appear to be induced in the shape of the major specular lobe at broadside.

In several instances, nulls between lobes have also been significantly reduced. In Pattern Set (b) of Figure 11, for example, the null near 65^{O} is changed by over 18 dB by giving various positions to the tree.

6. BACKSCATTER PHASE AND DUAL FREQUENCY PHASE SIGNATURES

The phase to be discussed in this section is that of the far-zone backscattered field at constant range. The quantity actually measured was the relative phase of a signal that traveled from the transmitter through the transmitting branch of the equipment and on to the scattering target, that was then modified by the scatterer and reflected back to the antenna, and that finally traveled through the receiving branch of the equipment to the second hybrid. This quantity was then subtracted from the corresponding value of a signal that traveled over the identical electrical paths and was reflected from a target of known scattering properties. All of the paths that were electrically identical for the two signals subtracted out of the results, leaving only phase differences between the target and the reference scatterer.

Dual frequency phase signatures given in Figures 14 and 16 are defined as

$$S_2 = 2\psi_L - \psi_H \tag{3}$$

where ψ_L is the measured phase of the far-zone backscattered field corresponding to the low frequency and ψ_H is that corresponding to the high frequency. Note that, for scatterers small compared to a wavelength, the Rayleigh-region phase is independent of frequency and Eq. (3) gives the phase itself.

The significance of dual frequency phase signatures is that two phase stable harmonically-related frequencies are practical for implementation in an actual radar, and when the backscattered phase as discussed here is measured from a scatterer at these two frequencies, the processing indicated by Eq. (3) removes all range-dependent and doppler-dependent phase changes, leaving a quantity dependent only on the phase of the scatterer.

Results are given for the three measurement planes shown in Figure 12. The center of rotation, or phase center, was chosen in each case to be midway between the ends of the models including the truck bumpers. For the vertical plane, it was also midway between the sides; for the side plane, it was midway between the top and bottom excluding the truck cab.

Curves in Figures 13 and 15 are labeled "High Frequency" and "Low Frequency." The "High Frequency" results are those measured with the 60-MHz model and the "Low Frequency" ones are those measured with the 30-MHz model.

The measured phase of the jeep model is given in Figure 13 and the corresponding dual frequency phase signatures are in Figure 14. Again, the front of the model was at or near 0° azimuth, with broadside near 90°.

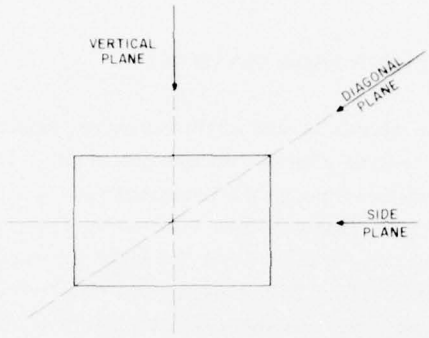

Figure 12. Planes of Phase Measurements

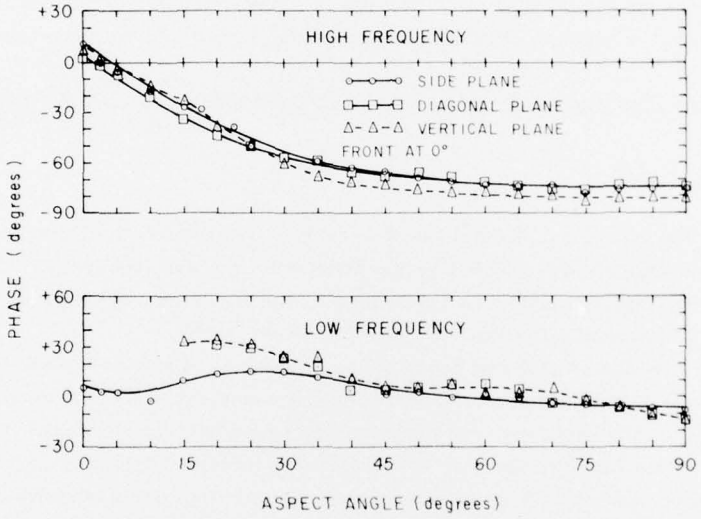

Figure 13. Measured Phase – Jeeps

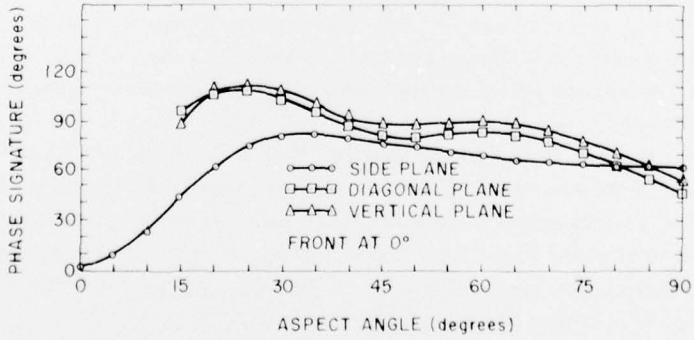

Figure 14. Dual Frequency Phase Signatures

Reflected signals from the 30-MHz jeep model were so low near the front and back directions that accurate phase measurements could not be made at aspect angles of less than about 45^{O}. The measured points shown in the lower part of Figure 13 within this region are included to illustrate the effect of errors on the true phase values. Additional measurements have shown that these curves should be straight lines through the 0^{O} aspect.

For the 60-MHz model, the curves are essentially identical for all three planes of measurement and show a large angular interval about broadside over which the phase is approximately independent of viewing direction. For example, there is less than a 10^{O} change in phase over a $\pm 45^{O}$ change in aspect about broadside. Beyond this region towards the endfire directions, the phase is nearly a linear function of the aspect angle, increasing from approximately -75^{O} to approximately $+5^{O}$ at endfire.

The dual frequency phase signatures of Figure 14 reflect the foregoing characteristics, including the regions of questionable accuracy. Results for the side plane of measurement appear to be most accurate, and here the signature function is basically two straight lines. The first line, extending from end-on directions to about 30^{O}, increases from near 0^{O} phase at 0^{O} azimuth to about 90^{O} phase at 30^{O} azimuth, indicating a slope of about 3^{O} change in phase per degree change in azimuth. The second line extending from 30^{O} azimuth to broadside drops from about 90^{O} phase at 30^{O} azimuth to about 60^{O} phase at 90^{O} azimuth, yielding a slope of -1^{O} phase change per azimuth degree.

Corresponding results for the truck are in Figures 15 and 16. Because of the reduced symmetry these patterns extend from 0^{O} to 180^{O} in azimuth for measurements in the side and diagonal planes. The vertical plane pattern is extended over a full 360^{O} to show differences in phase of the signal reflected from the planar bottom and more detailed top of the model. In the graphs, the curve for the vertical plane has been folded, with the top and bottom halves given separately as labeled.

As expected from the radar cross section curves, backscatter phase patterns for the 30-MHz truck are very similar to those of the 60-MHz jeep, except that the range of the former is generally less than the range of those for the jeep. Here again, the curves could be represented by simple functions or broken straight lines.

Results for the largest 60-Mc model show significant differences in the different planes and between the forward and backward directions. Over a conical region of approximately 90^{O} in the forward directions, the phase is essentially constant with an average value of -235^{O}. A similar region exists in backward directions, but here there are differences for the different planes, with the phase changing from -205^{O} in the sideplane to -170^{O} in the vertical plane. At broadside, the

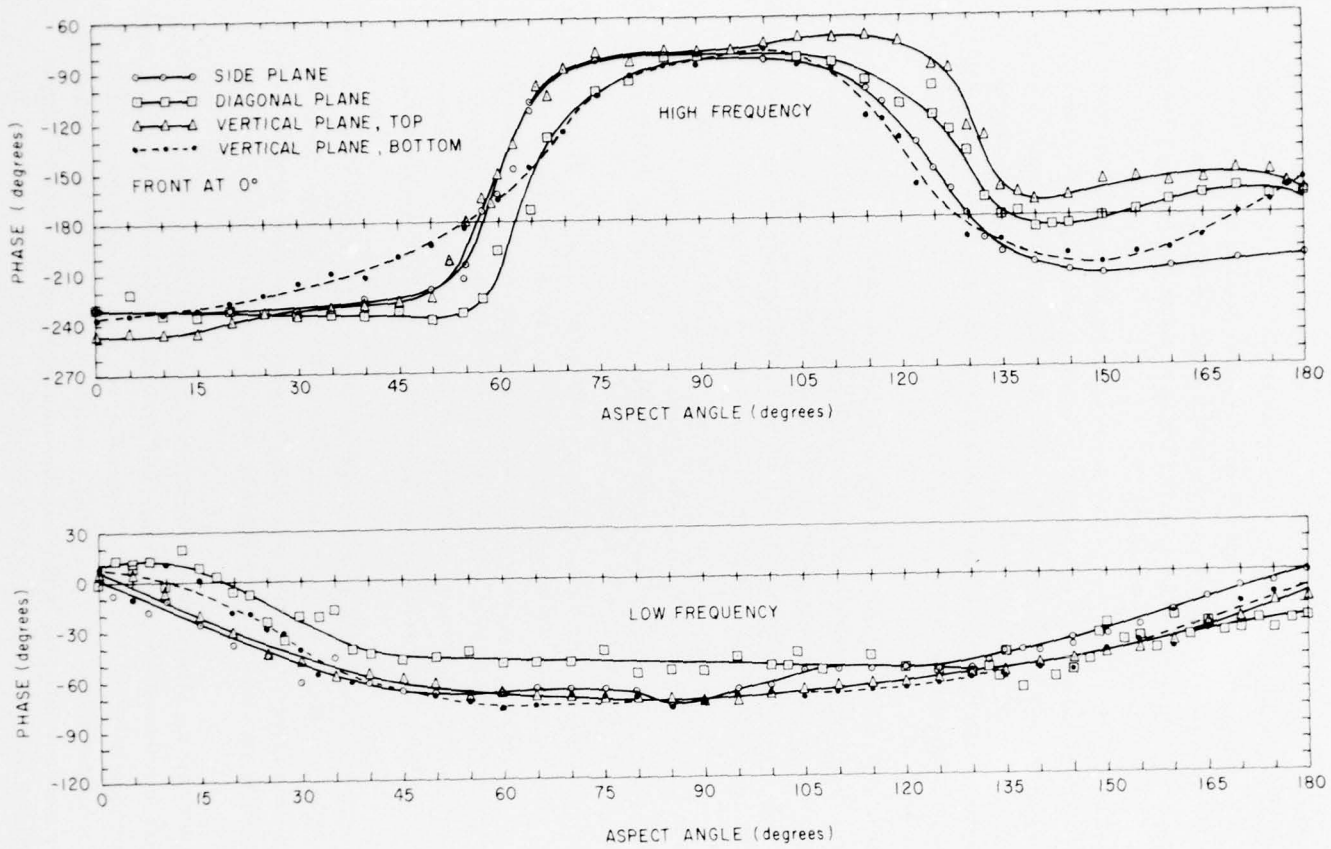

Figure 15. Measured Phase – 6 × 6 Trucks

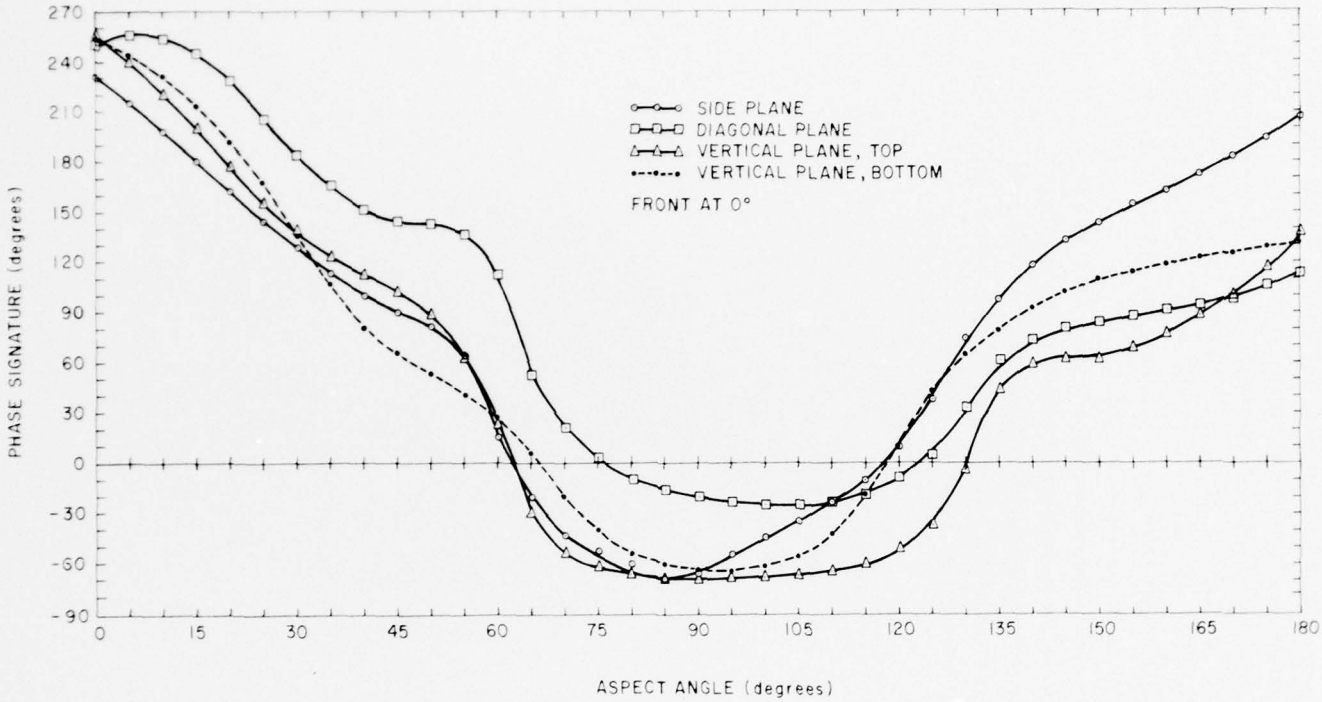

Figure 16. Dual Frequency Phase Signatures – 6 × 6 Trucks

phase in all planes reduces to about -80^{O}, but there is a rather limited region over which the phase approximates a constant value.

Principal differences between from the top of the model and from the bottom of the model patterns occur at the higher frequency and at the corresponding angles of 50^{O} and 230^{O}, 65^{O} and 245^{O}, 125^{O} and 305^{O}, showing that although the cab for this model is only about $\lambda/16$ above the body and $\lambda/8$ in extent, it introduces measurable perturbations to the phase.

The dual frequency phase signatures (Figure 16) vary over a total range of about 330^{O} from the forward direction to broadside, and there are significant differences between patterns in the different planes. The pattern variations are monotonic as functions of the aspect angle, however, and include a small region of near constant values about broadside.

References

1. Blacksmith, P., Hiatt, R.E., and Mack, R.B. (1965) Introduction to radar cross section measurements, Proc. IEEE 53:901-920.

2. Mack, R.B., Wojcicki, A.W., and Andriotakis, J.J. (1973) An Implementation of Conventional Methods of Measuring the Amplitude and Phase of Backscatter Fields, AFCRL-TR-73-0418.

3. Mack, R.B. (1971) Phase, Phase Signatures, and Simple Inverse Properties of Backscatter Fields from Thin Rods, AFCRL-TR-71-0526.

4. Mack, R.B. (1971) Phase properties of backscattered fields from thin rods, IEEE Trans. G-AP AP-19:450-451.

METRIC SYSTEM

BASE UNITS:

Quantity	Unit	SI Symbol	Formula
length	metre	m	...
mass	kilogram	kg	...
time	second	s	...
electric current	ampere	A	...
thermodynamic temperature	kelvin	K	...
amount of substance	*mole*	*mol*	...
luminous intensity	candela	cd	...

SUPPLEMENTARY UNITS:

plane angle	radian	rad	...
solid angle	steradian	sr	...

DERIVED UNITS:

Acceleration	metre per second squared	...	m/s
activity (of a radioactive source)	disintegration per second	...	(disintegration)/s
angular acceleration	radian per second squared	...	rad/s
angular velocity	radian per second	...	rad/s
area	square metre	...	m
density	kilogram per cubic metre	...	kg/m
electric capacitance	farad	F	A·s/V
electrical conductance	siemens	S	A/V
electric field strength	volt per metre	...	V/m
electric inductance	henry	H	V·s/A
electric potential difference	volt	V	W/A
electric resistance	ohm	...	V/A
electromotive force	volt	V	W/A
energy	joule	J	N·m
entropy	joule per kelvin	...	J/k
force	newton	N	kg·m/s
frequency	hertz	Hz	(cycle)/s
illuminance	lux	lx	lm/m
luminance	candela per square metre	...	cd/m
luminous flux	lumen	lm	cd·sr
magnetic field strength	ampere per metre	...	A/m
magnetic flux	weber	Wb	V·s
magnetic flux density	tesla	T	Wb/m
magnetomotive force	ampere	A	...
power	watt	W	J/s
pressure	pascal	Pa	N/m
quantity of electricity	coulomb	C	A·s
quantity of heat	joule	J	N·m
radiant intensity	watt per steradian	...	W/sr
specific heat	joule per kilogram-kelvin	...	J/kg·K
stress	pascal	Pa	N/m
thermal conductivity	watt per metre-kelvin	...	W/m·K
velocity	metre per second	...	m/s
viscosity, dynamic	pascal second	...	Pa·s
viscosity, kinematic	square metre per second	...	m/s
voltage	volt	V	W/A
volume	cubic metre	...	m
wavenumber	reciprocal metre	...	(wave)/m
work	joule	J	N·m

SI PREFIXES:

Multiplication Factors	Prefix	SI Symbol
1 000 000 000 000 = 10^{12}	tera	T
1 000 000 000 = 10^{9}	giga	G
1 000 000 = 10^{6}	mega	M
1 000 = 10^{3}	kilo	k
100 = 10^{2}	hecto*	h
10 = 10^{1}	deka*	da
0.1 = 10^{-1}	deci*	d
0.01 = 10^{-2}	centi*	c
0.001 = 10^{-3}	milli	m
0.000 001 = 10^{-6}	micro	μ
0.000 000 001 = 10^{-9}	nano	n
0.000 000 000 001 = 10^{-12}	pico	p
0.000 000 000 000 001 = 10^{-15}	femto	f
0.000 000 000 000 000 001 = 10^{-18}	atto	a

* To be avoided where possible.